Single Mol. **1** (2000) 1, 25-31

3D Imaging of Individual Ion Channels in Live Cells at 40 nm Resolution

Gerhard J. Schütz [a)], Vassili Ph. Pastushenko [a)], Hermann J. Gruber [a)], Hans-Günter Knaus [b)], Bernt Pragl [b)] and Hansgeorg Schindler [a)]

[a)] *Institute for Biophysics, University of Linz, Altenbergerstr.69, A-4040 Linz*
[b)] *Institute for Biochemical Pharmacology, University of Innsbruck, Peter-Mayr-Str.1, A-6020 Innsbruck*

Correspondence to
G. J. Schütz
Institute for Biophysics, University of Linz,
Altenbergerstr.69, A-4040 Linz, Austria,
Phone +43-732-2468-9265
Fax +43-732-2468-822,
e-mail gerhard.schuetz@jk.uni-linz.ac.at

submitted 06 Dec 1999
published 31 Jan 2000

Abstract

High affinity binding of fluorescence labeled hongotoxin ($HgTX_1$-Cy5) to the potassium channel $K_v1.3$ in T-lymphocyte cell membranes was utilized for imaging single ion channels optically, employing Single Dye Tracing (SDT). Binding sites were seen as single fluorescence peaks in cross-sections through the cell. Their number matched, at conditions of saturated binding, the number of sites expected from biochemical determination. By fitting the peaks to the point-spread-function, well approximated by a Gaussian distribution, resolution of channel positions to within ±40nm was obtained in all three dimensions. Within the focal plane (x-y plane) positional resolution is given by the accuracy of determining the peak position of the Gaussian. The positional resolution along the optical axis (z-direction) was obtained from the accuracy of estimating the position of minimum defocusing for a single molecule. For this, the width of the fluorescence peaks in consecutive images, taken at different degrees of defocusing, were shown to accurately match the theoretical prediction, yielding ~40nm accuracy of finding the z-position of the labeled channels.

This first visualization of individual membrane proteins in live cells by fluorescence labeled ligands with 40nm 3D positional resolution opens new perspectives for the study of cellular organization and processes at the molecular level.

Introduction

One main goal in cell biology is the in vivo determination of the local distribution of cellular components and its dynamical changes. While electron microscopy is used as standard methodology for high resolution studies on fixed samples, imaging of living cells using fluorescence microscopy is limited by optical diffraction, yielding a lateral and axial resolution of the order of ~$\lambda/2$ and ~1.5λ, respectively, with λ the wavelength of the emitted fluorescence [1]. Substantial enhancement of the resolution along the optical axis has been obtained by reducing the excitation and detection volume within the sample using scanning techniques like confocal microscopy [2,3] or two photon microscopy [4,5]. Still, typical values lie above 100nm.

A different approach for in vivo determination of local distributions of single molecules at even higher precision of ~50 nm is possible in the regime of very low concentrations <<1 molecule per resolution unit. In this regime, the accuracy in determining the lateral position of a single fluorescence labeled molecule is only limited by the signal-to-noise ratio, yielding typical values of ~50nm [6]. Evidence for this positional resolution was so far obtained for single molecules in 2-dimensional systems, which also allowed for studies of lateral diffusion [7], [6], imaging of ATP-binding

[8], [9], or of the rotation of sliding actin filaments [10], [11]. A notable exception was the 3D tracking of single dye molecules within a porous gel [12]. In that study, single fluorophores were excited by an evanescent field in close proximity to a glass slide; variations in the fluorescence intensity due to different locations within the evanescent field were used for determination of the z-coordinate. For living cells, however, that method is not generally applicable since only the bottom part of a cell can be studied due to the short range of the evanescent field of <200nm [13].

High positional resolution in the 10nm range has been obtained for membrane proteins by 2- or 3-dimensional single particle tracking, utilizing the high signal-to-noise ratio of 40nm gold particles or highly fluorescent latex beads linked to the molecules [14-22]. In the present study we extend fluorescence imaging to the ultimate limit of a single fluorescence labeled membrane protein in the plasma membrane of a small cell (Jurkat cell) and determine its x, y, and z-coordinate to within 40nm. This is the extension of a previous study on sufficiently flat parts of large cells, allowing for observation of the two-dimensional diffusion of single fluorescence labeled lipids within the plasma membrane [23]. The labeled protein studied is the voltage-gated potassium channel, $K_V1.3$, [24] present at a low concentration in the plasma membrane of the Jurkat cell [25]. The channel protein was fluorescence labeled by binding a high affinity peptidyl inhibitor, Hongotoxin (HgTX1, A19C mutant) which had been labeled on Cys19 with one Cy5 fluorophore [26]. This channel and its inhibition by HgTX1 is instrumental in analyzing Ca2+ homeostasis. Inhibition of the channel by HgTX1 prevents mitogen-induced elevations in cytosolic Ca2+ concentrations, and as a consequence, the release of interleucin (IL)-2 [27].

Experimental

Cell Culture

Jurkat cells (ATCC, clone E6) were cultured in RPMI 1640 medium without phenolred supplemented with antibiotics and 10% FCS in a humidified atmosphere (95 %) at 5 % CO_2 and 37°C. Cells were transferred every 4 days. For fluorescence labeling of $K_V1.3$, cells were incubated for ~1h with 500pM Hongotoxin covalently linked to Cy5 ($HgTX_1$-Cy5) [26]. This sample was used for 3D imaging directly, without perfusing out free $HgTX_1$-Cy5.

Microscopy

The apparatus, data acquisition and automatic data analysis system were used as described in detail [28]. In brief, samples were illuminated for 10ms by 633nm light from a dye-laser (Model 375B, Spectra Physics, CA) using a 100-times objective (PlanNeofluar, NA=1.3, Zeiss, Oberkochen, Germany) in an epi-fluorescence microscope (Axiovert 135TV, Zeiss). The laser beam was defocused to an area of 850µm^2 at a mean intensity of 1.2kW/cm^2, resulting in a homogenous illumination over the analyzed area of 10x10µm (<6% intensity modulations). Rayleigh scattered light was effectively blocked by appropriate filter combinations (645 DRLPO2, 670 DF40, Omega, HSPF-632.8-1.0, Kaiser Optical Systems, MI). Images were obtained by a liquid-nitrogen cooled slow-scan CCD-camera system (AT200, Photometrix, Tucson, AR, equipped with a TK512CB-chip, Tektronix) and stored on a PC.

For 3D imaging, samples were illuminated consecutively for 5ms at a delay of 20ms. Different defocusing was obtained by shifting the objective axially by 200nm using a piezo-driven nanopositioning system (PIFOC, Physik Instrumente, Germany).

Data Analysis

The 3D point spread function of the aparatus was determined from measurements on 30nm Cy5-labeled latex beads immobilized on a glass slide. Fluorescence peaks of latex beads and of single molecules were analyzed accordingly. A maximum-likelihood fit was performed for each defocusing, assuming a gaussian fluorescence distribution at position x, y, described by a width, σ, and an overall number of detected fluorescence photons, F. This was found to be a sufficiently good approximation of the exact diffraction pattern described by an Airy function. Estimations for the fit parameter σ, F, x, y, N, with N the average background noise, were drawn from images at different defocusing. The resulting average values of F, x, y, N were used as input for a second run of the fitting procedure, yielding σ as a function of the defocusing, δz.

Results and Discussion

For this first attempt to image an ensemble of individual membrane proteins in living cells, simultaneously and in real time for monitoring membrane-associated processes, the choice of an appropriate system appeared crucial. We chose the dye molecule Cy5 with red fluorescence in order to minimize the amplitude of cellular auto-fluorescence. This background contribution is unavoidably co-collected since simultaneous imaging requires wide-field illumination, not allowing for spatial filtering by confocal optics. As to the choice of a suitable cell and of a membrane protein which can be addressed by this dye most specifically, selectively and stoichiometrically we chose the ion channel protein $K_V1.3$ in Jurkat cells (T-lymphocyte leukemia cell line) which is of considerable pharmacological interest [29]. The homo-tetramer channel structure binds hongotoxin ($HgTX_1$) in 1:1 stoichiometry and with pM affinity [30]. $HgTX_1$ labeled (1:1) with Cy5 via a free cystein residue was shown not to interfere with binding [26]. The high water solubility of $HgTX_1$-Cy5 renders unspecific association to cell

membranes low and a most unlikely event at pM concentration.

After this choice of system and fluorescent tool we first addressed the principle question of the feasibility of imaging single $HgTX_1$-Cy5 molecules at the plasma membrane of the Jurkat cell.

Single molecule imaging on cells is feasible

Jurkat cells were incubated with the toxin ligand ($HgTX_1$-Cy5) at 500pM concentration at which the binding of the toxin to the $K_V1.3$-ion in the Jurkat cell is expected to be in saturation [30]. The cell under study was fully illuminated for 10 ms with laser light of 633nm wavelength for excitation of Cy5 fluorescence which was collected from cross-sections of the cell for imaging. Fig.1A shows a typical fluorescence image obtained from a focal plane at the center of the cell. A number of single fluorescence peaks is clearly resolved, localized at the cell membrane (indicated by the dashed yellow line). From isolated peaks in several such images we determined the integrated intensities by fitting the peaks to 2D-Gaussian profiles. This was found to be a good approximation of the 2D point spread function [7]. Intensity values fell on a narrow distribution (Fig.1B) with a mean of 114counts and a standard deviation of 24counts. This observation of single fluorescence signals with a unitary signal value provided a first line of evidence that the observed peaks originate from single toxin molecules ($HgTX_1$-Cy5) at the cell surface. The high sensitivity of detecting single molecules for 10 ms illumination was achieved by excitation in the red, where cellular autofluorescence is low, and by utilizing the high extinction coefficient of Cy5, which allows for high count rates even at the low illumination intensity of 1.2kW/cm^2. Three main contributions to background noise were distinguished. In the absence of labeled toxin, the background noise had a Gaussian width of σ_b ~7counts, with about equal contributions from auto-fluorescence of the cell and from readout noise of the CCD-camera (σ~5counts). In the presence of $HgTX_1$-Cy5, the background noise was found to increase slightly from σ_b ~7 to typically 9 counts (see dashed profile in Fig.1B and legend for details). This increase is attributed to the collection of out-of-focus fluorescence from labeled toxin molecules at the cell membrane away from the focal plane. This resulting figure for total background noise yields a signal-to-noise ratio of S/N = 114 / 9 = 12.7 at 10ms illumination which allows for the clear detection of single toxin molecules in the cell membrane as seen in Fig.1A.

The practical use of this capability of imaging single molecules in cell membranes much depends on the degree to which the 3D-positions of the molecules in the cell membrane can be determined.

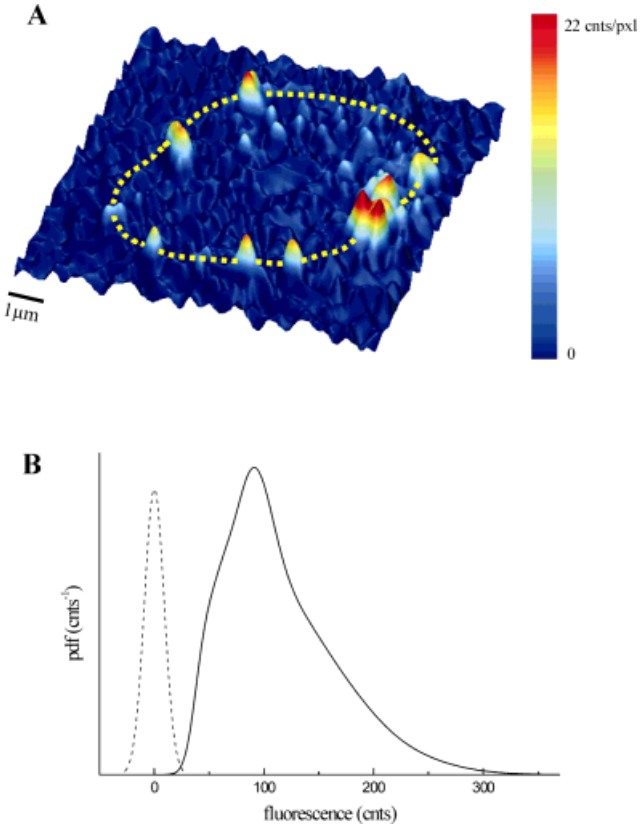

Fig. 1. *(A) Fluorescence image of a Jurkat cell after specific fluorescence labeling of the potassium channel $K_V1.3$ by $HgTX_1$-Cy5. The image shows an optical cross-section of the center of the cell. Individual fluorescence peaks are observed at the cell edge (dashed yellow line), and are attributed to the signal from single fluorescence labeled channel proteins. The signals at the right edge of the cell might indicate local clustering of channels. (B) For clear assignment of fluorescence signals to single molecules, the integrated fluorescence intensity of 24 isolated peaks were analyzed. The probability density yields a mono-modal distribution with a mean of 114 cnts. This mean has to be compared to the distribution of the background signal (dashed line), which was obtained from the background fluctuations within an area equal to the effective peak area. The standard deviation of 9cnts gives a signal to noise ratio for detecting single fluorophores of 114/9~13.*

Single molecules can be positioned within 40 nm in all three dimensions

In so-far studies using the SDT-method the labeled molecules were confined to planar 2D-systems (lipid membranes on planar substrates, for a review see [31]). This geometry rendered determination of the lateral positions of the single molecules straightforward by fitting the signals to 2D-Gaussian distributions, yielding a

resolution of typically 50nm for the position of single fluorophore molecules [6]. For the 3D-positioning of single molecules on cells one can use the same procedure for determining the lateral position of single molecules within the plane of illumination (x-y plane). However, the positioning along the optical axis (z direction) needed a new strategy of analysis. It was based on the principal fact that the width of the single peaks contains information about the distance between the molecule and the center of the focal plane. Inspection of single molecule peaks as seen in Fig.1A revealed, indeed, that the peaks considerably varied in width (Gaussian σ-width), while the integrated fluorescence intensity remained virtually the same (cf. Fig.1B). The latter observation is a consequence of using wide field illumination with virtually no intensity changes within the range of applied defocusing $-600nm \leq \delta z \leq 600nm$. However, the width of the point spread function for a defocused molecule ($\sigma(\delta z)$) is larger than for an in-focus molecule (σ_0). The z-dependence of the point spread function is very well described by $\sigma(\delta z) = \sigma_0 * (1 + (\delta z / d)^2)^{0.5}$, where d is the depth of focus and σ_0 the diffraction-limited width [32].

We first tested the validity of this relation for our experimental conditions by using 30nm sized polystyrene beads heavily labeled with Cy5, adsorbed to the surface of a glass slide in aqueous solution. Fluorescence images of individual beads were recorded for several positions of the focal plane, distant by $\delta z = 200nm$, for which the objective was shifted by a precision piezo-drive. The results are summarized in Fig.2. The integrated intensities remained, as expected, fairly constant for the seven 200nm spaced images (Fig.2 A). The σ-width values of the images (lower data set and left scale in Fig.2) followed well the predicted relation, as shown by the curve in Fig.2 B. Best fit indicated a focal depth of d = 411nm with an error of ± 30nm. The minimum value of the σ-width was $\sigma_0 = 205nm$ with an error of ± 7nm which is reasonably close to the diffraction-limit value of 140nm for the wavelength and objective used.

The apparent applicability of the relation between σ and δz for fluorescent beads was then used and put to a more refined test at the level of a single $HgTX_1$- Cy5 molecule in the Jurkat cell membrane. The experimental protocol was basically the same as for the beads, i.e. rise of the focal plane by 200nm steps with 5ms illumination for imaging at each focal plane and 20ms delay between the images. Fig.3 shows a series of 6 consecutive images (from A to F) of the same molecule, observed as in Fig.1A at the cell perimeter near the center of the cell. Gaussian fit to each image of the molecule yielded a fairly constant integrated intensity of (76 ±19) counts. The σ-width values of the six peaks, determined for constant integrated intensity of 76counts, are plotted in Fig.4. They are represented by the σ(δz)-relation almost as well as the data of the fluorescent beads (curve in Fig.4). Moreover, best fit yielded, within the given error margins, the same values for the parameters, $\sigma_0 = 193nm$ with an error of 12nm and d = 366nm with an error of 55nm. The errors represent the standard deviations of best fit for randomly chosen σ-values within the error bars of the data. This match of the σ(δz)-relation for single molecules and for beads provide confidence to the estimate of the single molecule position in the z-direction. It is obtained from the z-value at the minimum of the best fit yielding z = 498nm ± 31nm. The molecule is located, therefore, 498nm above the focal plane of image A in Fig.3, as one may roughly confirm by eye from the peak heights in Fig.3.

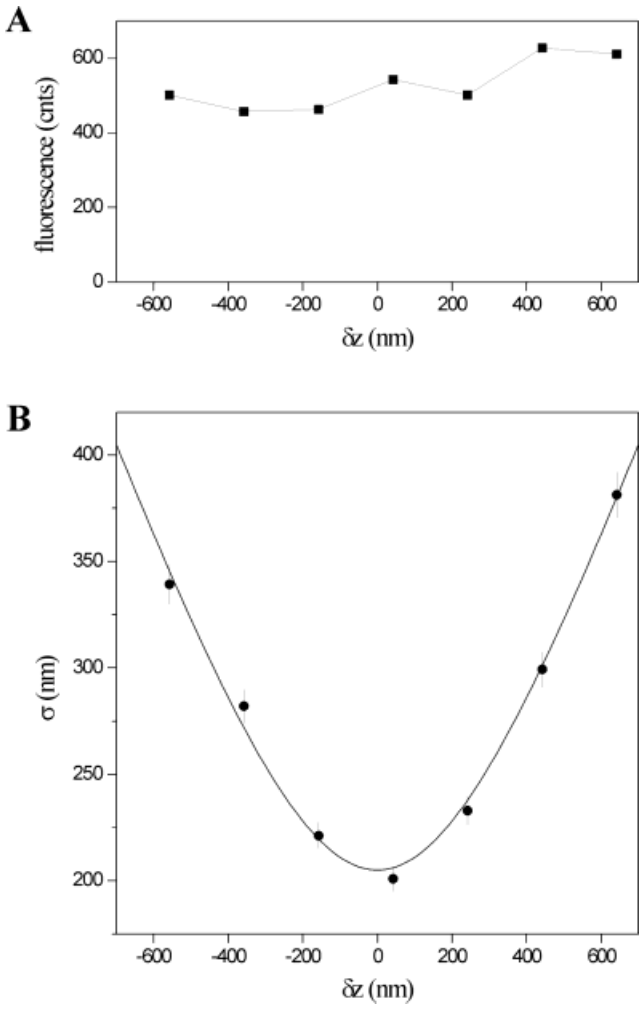

Fig. 2. *(A) Integrated fluorescence of a 30 nm Cy5-labeled polystyrene bead as a function of defocusing, δz. Values were determined for each optical cross-section from a 2-dimensional Gaussian fit. The fluorescence remains about constant over the whole range of defocusing, which ensures that both excitation intensity and detection efficiency are not altered by changes in δz. (B) Width of the point spread function of the beads as a function of defocusing. The data are fitted by a parabolic function (see text) described by a diffraction limited spot size σ0=205±7nm and a depth of focus d=411±30nm. The ordinate δz has been centered around the minimum, which was determined to an accuracy of ±16nm.*

The salient result is, however, that this procedure is quite robust in finding z-positions and with remarkable precision (31nm in the example of Fig.3-4). This accuracy well matches that in determining the lateral (x and y)-positions of the molecule within the plane of illumination which was about 40nm for the four highest peaks in Fig3.

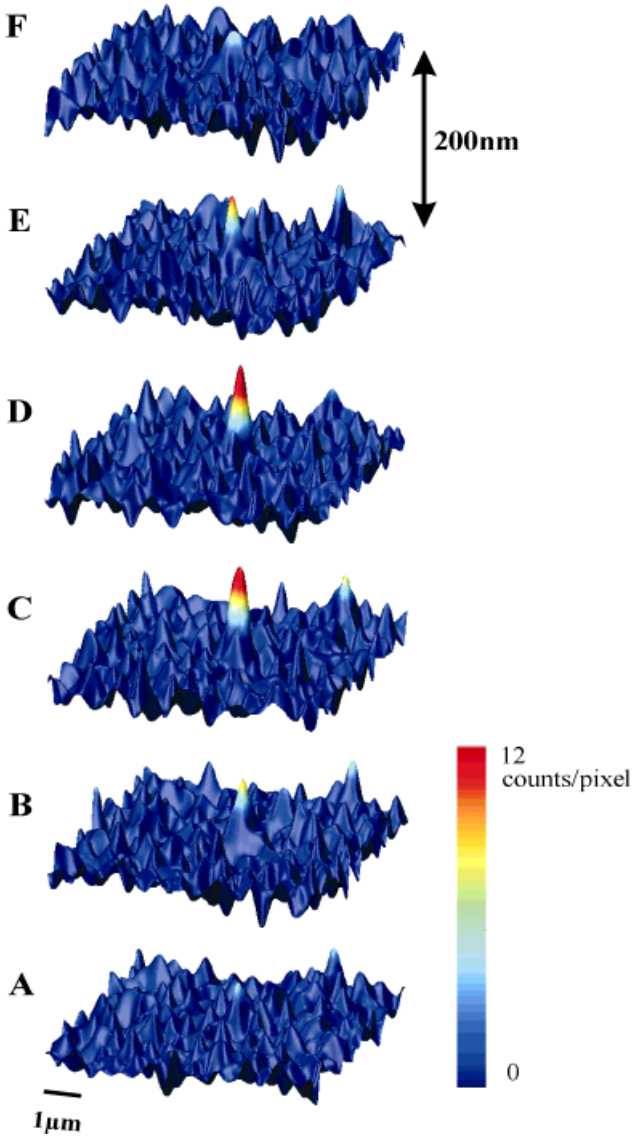

Fig. 3. *Consecutive imaging of a single fluorescence labeled potassium channel for different defocusing. The illumination time was 5ms for each of the 6 consecutive observations of the same molecule at different optical cross-sections with a defocusing of 200nm. The shape of the fluorescence peak varies with defocusing, yielding a small and broad signal at the bottom (A) and the top (F) image, and a high and sharp signal in the center images (C and D).*

Thus, consecutive 200nm z-shifts of the focal plane permit the determination of the 3D-position of a single molecule within 40nm in all three dimensions. It is to be noted that this is achieved at a rather low S/N ratio, of ~7 for the two highest peaks in Fig.3A, which permitted to take at least 10 images per dye before bleaching occurred.

This resolution of the position of a single molecule has to be distinguished from the minimum distance of 2 molecules to be still detected as isolated peaks, which is given by the diffraction-limited width, σ_0, in the x-y plane and by the focal depth, d, in the z-direction. 3D-Resolution of single molecule position, in contrast, depends on experimental parameters like S/N-ratio and the distance between consecutive focal planes. It was ~ 40nm in all 3 directions for the settings applied here.

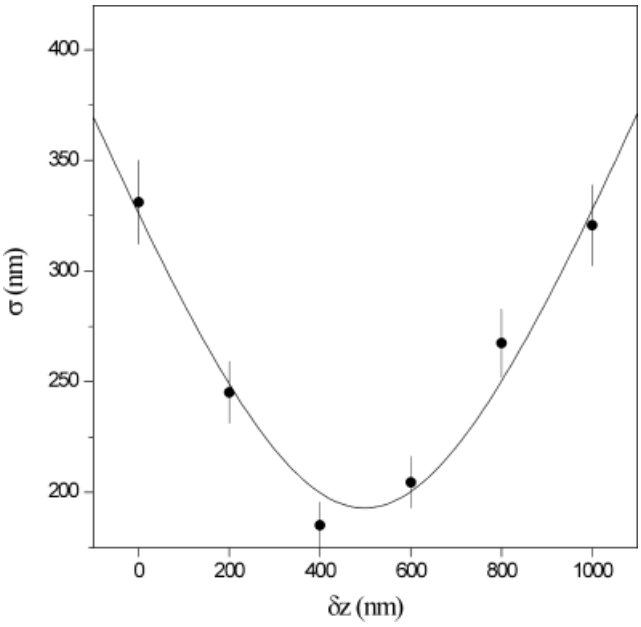

Fig. 4. *Width of the point spread function for the single molecule observed in Fig.3 as a function of defocusing. The data are fitted with a parabolic function described by a diffraction limited spot size σ0=193±12nm and a depth of focus d=366±55nm, which is in good agreement with the data obtained on 30nm latex beads (Fig.2). The z-coordinate of the molecule is calculated to be z=498±31nm.*

By knowing the resolution of single molecules in the z-direction, d ~ 400nm, one may estimate the surface density of the toxin label at the Jurkat cell membrane from the number of peaks in cross-sections. For the center cross-section in Fig.1 (radius R_{cell} ~ 4µm) the effective membrane area for resolving single molecules is $2\pi*R_{cell}*2d$ = 20µm^2 with ~ 12 $HgTX_1$-Cy5 molecules present, yielding a surface density of ~ 0.6 toxins /µm^2. This density of toxin should be equal to the density of $K_v1.3$ channels in the cell membrane, since the image was taken at conditions of saturated toxin binding. For the channel density a rough estimate can be obtained from the reported value of 20-120 fmole $HgTX_1$ binding sites per mg of Jurkat cell membrane

[25] and from a value of 10^{-11}mg/µm^2 for the mass density of the cell membrane, yielding ~ 0.1 to 0.7 channels/µm^2.

This match of the surface density of the labeled toxin with the density of high affinity binding sites, determined independently, leaves little doubt that the single peaks seen of unitary intensity are images of single labeled toxin molecules bound to K_v1.3 channel proteins in the cell membrane.

Characterizing lateral and rotational motion

The strategy of determining the z-position of a molecule by imaging at different focal planes can be used simultaneously for analyzing the mode of motion of the molecule. The data in Fig.3 represent a simple example. The described Gaussian fits of the six peaks revealed that the peak positions in the x-y plane were virtually the same for all peaks. More specifically, their best fit positions deviated from the average position of the 6 peaks by a standard deviation of 40nm, which is within the resolution of each position of also 40nm. Since the maximum time lag was 100ms, one may estimate an upper limit for the diffusion constant of the molecule, from $D_{lat} < (40nm)^2 / (4*0.1s) = 4x10^{-11}cm^2/s$. This value suggests that the labeled K_v1.3 channel might be immobilized rather than freely diffusing. Indeed, the measurement had been repeated after 2.5s, for which the molecule was still found at the same place within positional accuracy, reducing the limit to $D_{lat}<2x10^{-12}cm^2/s$, which safely indicates immobilization of the channel.

It should be added that free diffusion of a membrane protein between consecutive observations might interfere with the z-resolution of the described method. Using fastest acquisition of the data set (cf. Fig.3), however, this effect of diffusion can be reduced. For example, the expected displacement of a membrane protein in z-direction during a delay time of only 10ms would equal z-resolution of 40nm for a diffusion constant of $8x10^{-10}cm^2/s$. Since most membrane proteins show slower diffusion [32], the method for 3D-positioning appears applicable also to dynamic systems.

Finally, the data presented clearly show that the Cy5-label on $HgTX_1$ undergoes random rotational diffusion, as it was expected from the flexible spacer (14 mostly single bonds) between Cy5 and toxin [26]. The excitation light was linearly polarized in the x-direction, so that, for the center cross-section of Fig.1, any significant deviation from random rotational diffusion would have led to strong and systematic variations of the integrated peak intensity along the perimeter of the cell. There was no indication for such a variation for all peaks analyzed at different relative orientations along the cell perimeter (cf. Fig.1A and B).

Vice versa, analysis of integrated intensity along the perimeter can be instrumental for identifying and quantification of anisotropy in the rotational motion of the fluorescence label, or when it is rigidly coupled, of the labeled membrane component.

Conclusions and Perspectives

From the data we conclude, that it is well possible to detect single fluorescent toxin ligands ($HgTX_1$-Cy5) at the surface of a Jurkat cell membrane, specifically bound to K_v1.3 channel structures. The positions of the labeled channels are resolvable to ±40nm in all three directions.

It was also indicated that the mode of lateral motion of the channels can be analyzed as well as the mode of rotational motion as well as the distribution of channels including co-localization. The binding of the labeled toxin may be quantified by dose-response curves, with differentiation as to the state of channel mobility, association or location in the membrane. This potential opens a whole scenario of studies promising new insights, valuable for basic pharmacology and for the drug finding process. The data also indicate that receptor mapping over whole cell membranes at nearly real time may be feasible by shifting the focal plane through the whole cell which would add a new dimension to cell-physiology studies.

Acknowledgement We would like to thank H. Kahr for running the cell culture. This work was supported by the Austrian Ministry of Science, projects GZ 200.027/2 and GZ 200.027/3, by the Austrian Research Funds, P12803-MED, and by the EC-BIOTECHNOLOGY program project ERBBIO4CT960592

References

[1] Inoué, S. in Handbook of biological confocal microscopy, J.B.Pawley, Ed., Plenum Press, New York and London (1995) 1
[2] Minsky, M. Scanning **10** (1988) 128
[3] Pawley, J. B. Handbook of biological confocal microscopy. Plenum Press, New York and London, (1995)
[4] Denk, W., Strickler, J. H., Webb, W. W. Science **248** (1990) 73
[5] Denk, W., Piston, D. W., Webb, W. W. in Handbook of biological confocal microscopy, J.B.Pawley, Ed., Plenum Press, New York and London (1995) 445
[6] Schütz, G. J., Schindler, H., Schmidt, Th. Biophys.J. **73** (1997) 1073
[7] Schmidt, Th., Schütz, G. J., Baumgartner, W., Gruber, H. J., Schindler, H. Proc.Natl.Acad.Sci. **93** (1996) 2926
[8] Funatsu, T., Harada, Y., Tokunaga, M., Saito, K., Yanagida, T. Nature **374** (1995) 555

[9] Ishijima, A., Kojima, H., Funatsu, T., Tokunaga, M., Higuchi, H., Tanaka, H., Yanagida, T. Cell. **92** (1998) 161
[10] Sase, I., Miyata, H., Corrie, J. E. T., Craik, J. S., K.Kinosita Jr. Biophys.J. **69** (1995) 323
[11] Sase, I., Myata, H., Ishiwata, S., K.Kinosita Jr. Proc.Natl.Acad.Sci.USA **94** (1997) 5646
[12] Dickson, R. M., Norris, D. J., Tzeng, Y.-L., Moerner, W. E. Science **274** (1996) 966
[13] Gingell, D., Heavens, O. S., Mellor, J. S. J. Cell Sci. **87** (1987) 677
[14] Barak, L. S., Webb, W. W. J. Cell Biol. **90** (1981) 595
[15] Gelles, J., Schnapp, B. J., Sheetz, M. P. Nature **331** (1988) 450
[16] Anderson, C. M., Georgiou, G. N., Morrison, I. E. G., Stevenson, G.V.W, Cherry, R. J.Cell Sci. **101** (1992) 415
[17] Lee, G. M., Ishihara, A., Jacobson, K. Proc.Natl.Acad.Sci.USA **88** (1993) 6274
[18] Kusumi, A., Sako, Y., Yamamoto, M. Biophys.J. **65** (1993) 2021
[19] Ghosh, R., Webb, W. W. Biophys.J. **66** (1994) 1301
[20] Peters, I. M., de Grooth, B. G., Schins, J. M., Figdor, C. G., Greve, J. Rev.Sci.Instrum. **69** (1998) 2762
[21] Pralle, A., Prummer, M., Florin, E.-L., Stelzer, E. H. K., Hörber, J. K. H. Microscopy Research and Technique **44** (1999) 378
[22] Saxton, M., Jacobson, K. Ann.Rev.Biophys.Biomol.Struct. **26** (1997) 373
[23] Schütz, G. J., Kada, G., Pastushenko, V. Ph. Schindler, H. submitted
[24] Kaczorowski, G. J., Garcia, M. L. Curr.Opin.Chem.Biol. **4** (1999) 448
[25] Helms, L. M. H., Felix, J. P., Bugianesi, R. M., Garcia, M. L., Stevens, S., Leonard, R. J., Knaus, H.-G., Koch, R., Wanner, S. G., Kaczorowski, G. J., Slaughter, R. S. Biochemistry **36** (1997) 3737
[26] Koschak, A., Pragl, B., Darbon, H., Gruber, H. J., Schütz, G. J., Gerster, U., Knaus, H.-G. submitted
[27] Price, M., Lee, S. C., Deutsch, C. Proc.Natl.Acad.Sci.U.S.A **86** (1989) 10171
[28] Schmidt, Th., Schütz, G. J., Baumgartner, W., Gruber, H. J., Schindler, H. J.Phys.Chem. **99** (1995) 17662
[29] Leonard, R. J., Garcia, M. L., Slaughter, R. S., Reuben, J .P. Proc.Natl.Acad.Sci.U.S.A. **89** (1992) 10094
[30] Koschak, A., Bugianesi, R. M., Mitterdorfer, J., Kaczorowski, G. J., Garcia, M. L., Knaus, H.-G. J.Biol.Chem. **273** (1998) 2639
[31] Schmidt, Th., Hinterdorfer, P., Schindler, H. Microscopy Research and Technique **44** (1999) 339
[32] Weber, H. in Bergmann – Schaefer Lehrbuch der Experimentalphysik – Optik, H.Niedrig, Ed., Walter de Gruyter, Berlin and New York (1993) 755
[33] Edidin, M. in The structure of biological membranes, P.Yeagle, Ed., CRC Press, Boca Raton, Fl. (1992) 539